Maximizing the Electromagnetic and Chemical Resonances of Surface-Enhanced Raman Scattering for Nucleic Acids

Lindsay M. Freeman, Lin Pang, and Yeshaiahu Fainman*

Department of Electrical and Computer Engineering, University of California San Diego, 9500 Gilman Drive, La Jolla, California 92093-0407, United States

ABSTRACT Although surface-enhanced Raman spectroscopy (SERS) has previously been performed with nucleic acids, the measured intensities for each nucleic acid have varied significantly depending on the SERS substrate and excitation wavelength. We have demonstrated that the charge-transfer (CT) mechanism, also known as the chemical enhancement of SERS, is responsible for the discrepancies previously reported in literature. The electronic states of cytosine and guanine attached to silver atoms are computationally calculated and experimentally measured to be in the visible range, which leads to a resonance Raman effect at the corresponding maximum wavelengths. The resulting SERS measurements are in good agreement with the simulated values, in which cytosine-silver shows stronger enhancement at 532 nm and guanine-silver shows stronger enhancement at 785 nm. An atomic layer of aluminum oxide is deposited on substrates to prevent charge-transfer, and corresponding measurements show weaker Raman signals caused by the suppression of the chemical resonance. These findings suggest the optimal SERS signal can be achieved by tuning the excitation wavelength to match both the electromagnetic and chemical resonances, paving the way for future single molecule detection of nucleic acids other than adenine.

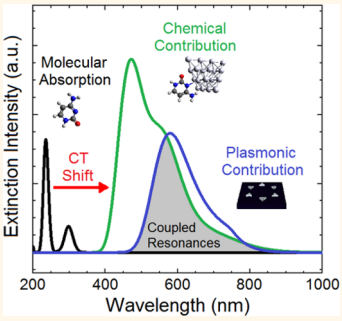

KEYWORDS: surface-enhanced Raman spectroscopy · charge-transfer effect · chemical resonance · plasmonic resonance · nucleic acids

Despite the reported achievement of the $1000 genome,[1] there remains a need for lower cost, higher throughput, and more accurate DNA sequencing that will minimize reagent costs, manual labor, and expensive instrumentation. While a variety of DNA sequencing methods currently exists on the open market, at present there are no methods that utilize Raman spectroscopy, a tool that holds enormous potential as a label-free identification probe of nucleic acid sequences. A Raman based DNA sequencing approach would not require large biomolecules such as polymerase or ligase and, thus, would simplify the sample preparation and reduce the material costs. Although preliminary studies have been conducted on analyzing the composition of DNA strands with Raman spectroscopy, they have failed to successfully propose how detection of sequences would be realized.

Surface-enhanced Raman scattering (SERS) has long been expected to be a label-free identification probe of nucleic acid sequences since a large number of SERS substrates with consistent local field enhancements for improved chemical detection have been designed and fabricated (metal nanoparticles,[2−4] nanoplasmonic resonators,[5−7] *etc.*). However, the experimental outcomes have been discouraging as the four bases of DNA (adenine, cytosine, guanine, and thymine) gave far different Raman intensity signals[8] and adenine was the only base that demonstrated single molecule SERS (SM-SERS),[9] making Raman sequencing seemingly impossible. More importantly, signal domination from bases have changed from experiment[10] to experiment,[11] with different excitation wavelengths showing extreme variance of the measured Raman intensities and the Raman intensity never correlating to the concentration of the bases.[12] Multiple explanations had been provided for these discrepancies, ranging from the magnitude difference of the Raman cross sections of the bases[13] to the orientation of the molecules on

* Address correspondence to fainman@eng.ucsd.edu.

Received for review May 27, 2014 and accepted July 25, 2014.

Published online July 28, 2014
10.1021/nn5028664

© 2014 American Chemical Society

the substrate leading to nonresonant enhancement.[12] The conclusion was drawn that determining a DNA sequence with SERS was unrealistic due to this inability in accurately measuring the SERS signature of nucleic acids. Although there are many challenges we face before realizing a Raman based DNA sequencing method, such as spatial resolution and poor signal-to-noise ratio (SNR), we must first resolve why there have been inconsistencies in SERS measurements of the DNA bases.

In this manuscript, we report our findings on why there have been repeated discrepancies regarding the surface-enhanced Raman signal of DNA bases. We hypothesize that the differences in SERS nucleic acid intensities at different excitation wavelengths are caused by the charge-transfer (CT) effect that leads to resonance Raman scattering (RRS). Using cytosine and guanine as examples, we first perform density-functional theory (DFT) calculations to determine the electronic transitions created between silver atoms and cytosine and guanine, and observe a clear shift as the absorption changes from the UV range for the base to the visible range for the base metal system. We then verify the new absorption spectra using optical absorption measurements.[14] The resonance dependence on the electronic transition shift of cytosine and guanine metal systems reveal strong wavelength-dependent behavior of SERS signals. By matching plasmonic resonances of SERS substrates to the shifted electronic transitions of cytosine and guanine conjugated to the metal surface, we verify that the SERS signals can be modulated by selecting the appropriate excitation wavelength. Furthermore, we use a thin layer of aluminum oxide to prevent electron transfer and thus remove the resonance CT band, and then experimentally validate our results with SERS measurements to predict the chemical enhancement factor. In doing so, we are the first to show that a DNA base SERS system's intensities are dependent on the excitation energy and is caused by the CT resonant band that is created by the transfer of electrons between the metal and nucleic acid.

RESULTS AND DISCUSSION

Time-dependent density functional theory (TD-DFT) studies on the absorption properties of metal atom clusters with attached molecules have been previously utilized for understanding the charge-transfer effect that leads to a chemical enhancement when the excitation energy is resonant with the electronic transition.[15,16] The studies that have been done on the chemical enhancement effect have used simple molecules such as pyridine[15] or benzenethiol,[17] and TD-DFT studies on nucleic acids primarily have been focused on geometrical adsorption studies with silver and adenine.[18,19] To calculate what electronic transitions are created when cytosine and guanine bind to silver atoms that lead to chemical enhancement in SERS, we perform TD-DFT simulations to measure the electronic transitions and relate the results to the chemical enhancement occurring in SERS experiments.

TD-DFT simplifies density-functional theory to a time-dependent situation in which the system is exposed to a time-dependent perturbation, causing a change in the system's external potential. By measuring the response of the charge density to a perturbation, the oscillator strengths and transition energies can be calculated, in which the oscillator strength is defined as the probability of absorption between the energy levels of the molecule.[20] TD-DFT energy level calculations (Figure 1) are performed on cytosine, guanine, cytosine−silver (C−Ag), and guanine−silver (G−Ag) using the Gaussian 09 software. Geometry optimization, in which atoms are repositioned until reaching an energy minimum, is performed on each system before TD-DFT calculations are used to ensure the systems are stable with no imaginary frequencies.[21] The silver cluster model chosen for the calculations is the 20-atom silver tetrahedral structure, as this has shown to have similar electronic properties as silver nanoparticles used in experiments.[15−17] On the basis of previous comparisons of simulations to experimental results, the flat side of the structure is chosen in which the molecule binds to the (111) surface of the Ag_{20} face-centered cubic (fcc) lattice structure. The atom of the nucleic acid (N atom), which binds to the silver cluster, is determined during the geometric optimization simulation and correlates well to previous studies regarding the optimal binding site of nucleic acids to silver atoms.[22]

As expected, the UV−visible absorptions for both cytosine (Figure 1c, with a peak at wavelength of 235 nm) and guanine (Figure 1c, with a peak at wavelength of 263 nm) are in the ultraviolet range as these are the natural electronic transitions of the molecules. However, when the nucleic acids are attached to the silver cluster, the absorption shifts into the visible range for C−Ag (Figure 1d, with a peak at wavelength of 472 nm) and G−Ag (Figure 1d, with a peak at wavelength of 609 nm), respectively. The change in the absorption maxima corresponds to a change in the electronic transitions of the systems, showing that new charge-transfer bands are created between the Fermi energy level of the metal and the highest occupied molecular orbital (HOMO) of the nucleic acids (Figure 1e). To confirm the calculated C−Ag and G−Ag electronic transitions, optical absorption measurements are performed on thin 20 nm Ag films with cytosine, guanine, and a mixture functionalized to the surface (Figure 1f). The measured C−Ag CT band (green) and G−Ag CT band (red) absorption intensity maxima occur at wavelengths of 566 and 662 nm, respectively. A Mix-Ag CT is also recorded (black), and correlates well to when the experimental measurements of C−Ag and

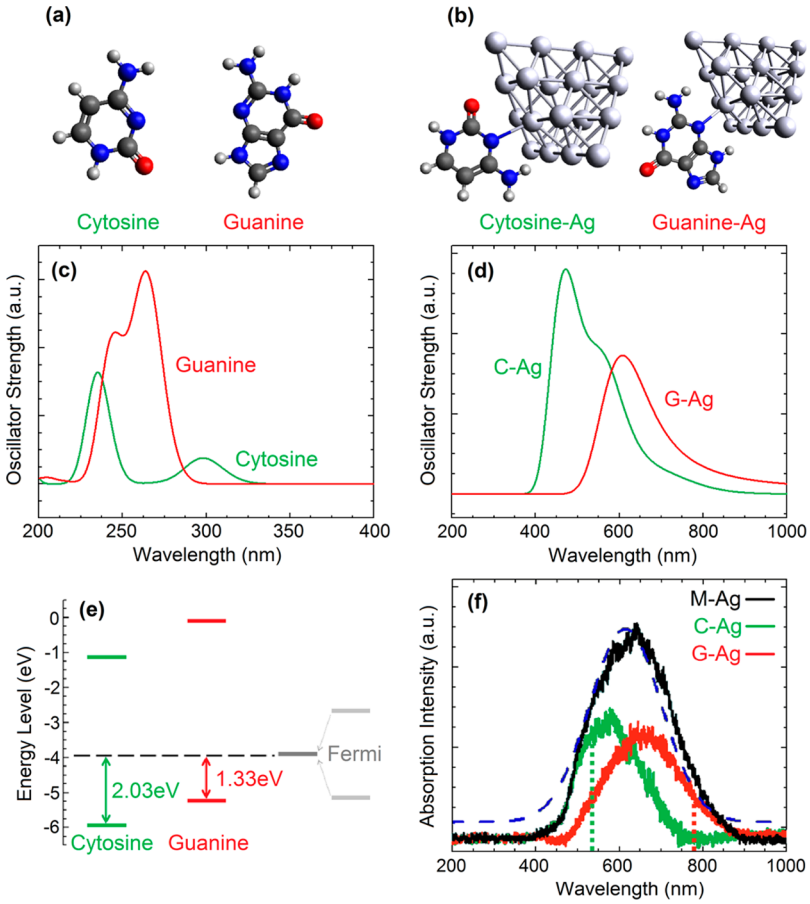

Figure 1. TD-DFT calculations of nucleic acids and nucleic acid silver systems geometrically optimized (a and b), showing the UV–vis absorption spectra of cytosine and guanine (c) and C–Ag and G–Ag (d). Cytosine and guanine have optical absorptions in the ultraviolet range, as expected based on previous experimental and simulation results. The addition of silver generates new electronic transitions in the visible range, with maximum oscillation strengths at 472 and 609 nm for C–Ag and G–Ag, respectively. (e) The electronic transitions created during electron transfer between the HOMO of the molecule and the Fermi energy of the silver. (f) Optical absorption measurements of cytosine (green), guanine (red), and mixture (black) on 20 nm Ag thickness, with values of 566 and 662 nm for C–Ag and G–Ag, respectively. The addition of C–Ag and G–Ag measurements is represented by the blue dotted line. The Raman excitation wavelengths (532 and 785 nm) are marked by the vertical dotted lines.

G–Ag are combined (blue dotted line). The experimentally measured absorption spectra show that the CT bands corresponding to the experimental data are fairly consistent with the absorption spectra simulations (Figure 1c,d). However, there are some differences in the simulation results and experimental measurements because only one adsorption configuration is used for the absorption band calculations. First, the experimental measurements show a red-shift of peak wavelength by 94 nm for C–Ag (simulation peak at wavelength of 472 nm, experimental peak at wavelength of 566 nm) and 53 nm for G–Ag (simulation peak at wavelength of 609 nm, experimental peak at wavelength of 662 nm). Second, using only one adsorption configuration results in narrower absorption bands ($fwhm_{C-Ag}$ = 161 nm, $fwhm_{G-Ag}$ = 135 nm) as opposed to experimental results ($fwhm_{C-Ag}$ = 192 nm, $fwhm_{G-Ag}$ = 204 nm) (fwhm: full-width half maxima). It is expected that additional adsorption configurations, such as attachment of the nucleic acid atom to the vortex of the silver atom cluster rather than to the surface face, or attachment *via* atoms other than the nitrogen ring atoms, would lead to shifts in the absorption bands. The convolution of the calculated absorption bands of all adsorption configurations would lead to the simulation results matching the experimental measurements. For this reason, the measured experimental results are assumed to be more representative of the CT bands of the system as opposed to the simulation results.

The regions where C–Ag and G–Ag show strong oscillation strength and absorption intensities correlate to the new electronic transitions created by the charge-transfer between the metal and nucleic acids. The optical absorption spectra have fwhm of ~250 nm, in which case there will be a chemical enhancement mechanism occurring between approximately 441 and 691 nm for C–Ag and 537 and 787 nm for G–Ag. From these results, we can substantiate our hypothesis that the enhancement difference found between the two nucleic acids in previously published

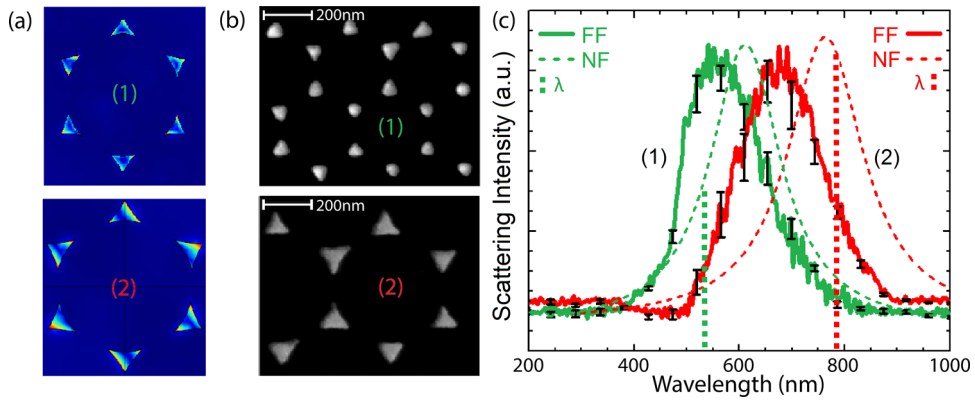

Figure 2. (a) COMSOL simulations of substrate #1 (300 nm bead mask, 75 nm side length, 45 nm thickness) and of substrate #2 (500 nm bead mask, 135 nm side length, 60 nm thickness). (b) SEM images of substrates. (c) Localized surface plasmon resonance scattering far field (FF) spectra of substrate #1 (green line, λ_{LSPR} = 569 nm) and substrate #2 (red line, λ_{LSPR} = 679 nm) and near field (NF) spectra of substrate #1 (green dashed line, λ_{NF} = 622 nm) and of substrate #2 (red dashed line, λ_{NF} = 763 nm). The excitation wavelengths for the SERS experiments are represented by the green (532 nm) and red (785 nm) vertical dotted lines. Error bars represent the scattering intensity deviation of the 5 LSPR measurements recorded.

results was caused by the induced Raman scattering in different excitation wavelengths used in the experiments, rather than by the difference in Raman-cross sections or orientation of the molecules.

To demonstrate the effect charge-transfer bands have on enhanced Raman signals when in resonance with the excitation wavelength, surface-enhanced Raman spectroscopy is performed with nucleic acids functionalized on silver islands. Due to experimental constraints, the laser wavelengths chosen are 532 and 785 nm (marked in Figure 1f, vertical dotted lines). On the basis of optical absorption measurements shown in Figure 1f, the 532 nm excitation wavelength will show strong chemical resonance of C−Ag and weak chemical resonance of G−Ag, while the 785 nm excitation wavelength will demonstrate no chemical resonance of C−Ag and weak chemical resonance of G−Ag. The silver island films are fabricated in such a way that their plasmonic resonance, which leads to a local electric field enhancement, is in the same wavelength range as the Raman excitation wavelength. In this way, both the plasmonic electromagnetic enhancement and charge-transfer chemical enhancement will be resonant in the same wavelength range, offering the maximum possible resonance Raman effect with the appropriate wavelength selection.

Silver island films are chosen as SERS substrates because they offer highly controllable, uniform, and reproducible surfaces that can be tuned for electromagnetic enhancement at any wavelength using Nanosphere Lithography (NSL).[23] Two substrates are designed: substrate #1 has a 300 nm bead mask (75 nm side length) and a 45 nm silver thickness and substrate #2 has a 500 nm bead mask (135 nm side length) and a 60 nm silver thickness. Finite element modeling (FEM) simulations are performed (COMSOL Multiphysics software package) to calculate the local electric field enhancement of both substrates (Figure 2a). Simulations show strong field enhancement at the tips of the silver islands. The corresponding SEM images of substrate #1 and #2 are shown in Figure 2b. For the silver island films to enhance the Raman signal, the two substrates must support localized surface plasmon resonances (LSPR) that lead to local electric field enhancement. The wavelength range in which the silver island films support the LSPR depends on the size and shape of the silver particles and can be determined by measuring the scattering of the particles with broadband excitation. The scattering spectra for the two silver island film substrates are shown in Figure 2c, with a larger feature size for substrate #2 leading to a red-shift of the λ_{LSPR}.

When we use the above fabricated silver island film as the substrates for DNA (*e.g.*, cytosine, guanine) Raman measurements, both the chemical enhancement from the induced resonance Raman from C−Ag or G−Ag and the electromagnetic enhancement from the LSPR would contribute to the total Raman scattering signal. By measuring the intensity of the absorption of the nucleic acid silver systems (Figure 1f) and the scattering of the LSPR from the pure silver island films (Figure 2c), the respective chemical enhancement and electromagnetic enhancement contributions can be estimated.

For calculating the electromagnetic contribution, the near field intensity distribution should be considered. The scattering results shown in Figure 2c in green and red (solid lines) are actually far field measurements. Fortunately, it is known that the far field spectra response deviates from the near field spectral distribution due to internal and radiative damping,[24] in which the near field local intensity enhancement maximum is red-shifted from the far field LSPR measurement. Using the model based on damped harmonic oscillators,[25] we calculate the damping factor for substrates #1 and #2. The damping factor (β) is found using the relationship

TABLE 1. Chemical and Plasmonic Contributions for the SERS Excitation Wavelengths of 532 and 785 nm, with the Intensities Normalized with the Total Maximum of the Two Contributions

	chemical contribution	plasmonic contribution	total
532 nm C—Ag	0.48	0.39	0.87
532 nm G—Ag	0.21	0.39	0.60
785 nm C—Ag	0	0.75	0.75
785 nm G—Ag	0.25	0.75	1

$\beta = w/(2\pi)$, where w is the fwhm of the Lorentzian fit of the far field measurements. The red-shifted near field ω_{NF} is then calculated from $\omega_{NF} = (\omega_0{}^2 - \beta^2/2)^{1/2}$. The damping effect leads to near field resonant wavelengths of 622 and 763 nm from far field resonant wavelengths of 569 and 679 nm, for substrates #1 and #2, respectively. The shifted near field intensity spectra are shown in Figure 2c (dashed lines).

The results of the chemical and electromagnetic contributions based on the absorption intensities and LSPR intensities with near field red-shift corrections are shown in Table 1, with the intensities normalized to the maximum total contribution (G—Ag on substrate #2 at 785 nm). For example, the absorption intensity for 532 nm C—Ag is 203 au and the scattering intensity is 164 au, resulting in chemical and plasmonic contributions of 0.48 and 0.39, respectively. From the total contribution estimation, we expect to see the Raman enhancement results at 532 nm to be C—Ag > G—Ag and at 785 nm to be G—Ag > C—Ag.

Raman spectroscopy is performed at 532 and 785 nm for C—Si, G-Si, C—Ag, and G—Ag, where concentrated cytosine and guanine are functionalized on silicon for SERS comparison to normal Raman scattering (NRS). For analysis, the ring-breathing modes (RBM) of cytosine and guanine (~790 and ~650 cm^{-1}, respectively), the single bond stretching modes (SSM) of cytosine and guanine (~1290 and ~1230 cm^{-1}, respectively), and the double bond stretching modes (DSM) of cytosine and guanine (~1650 and ~1550 cm^{-1}, respectively) are selected for analysis as these are the standard modes used for DNA Raman spectroscopy measurements.[12,13]

With an excitation wavelength of 532 nm on substrate #1 (Figure 3a), cytosine (C—Ag) is shown to have a stronger surface-enhanced Raman signal than guanine (G—Ag) based on the RBM, SSM and DSM. The bulk Raman signals of cytosine (C—Si) and guanine (G—Si) functionalized on a clean silicon wafer are also taken for comparison, showing that the NRS signals have consistent intensities between the two nucleic acids at both wavelengths. The results are directly opposite for an excitation wavelength of 785 nm on substrate #2 (Figure 3b), in which the surface-enhanced signals of the RBM, SSM, and DSM for substrate #2 of G—Ag are shown to be larger than those of C—Ag due to the signal

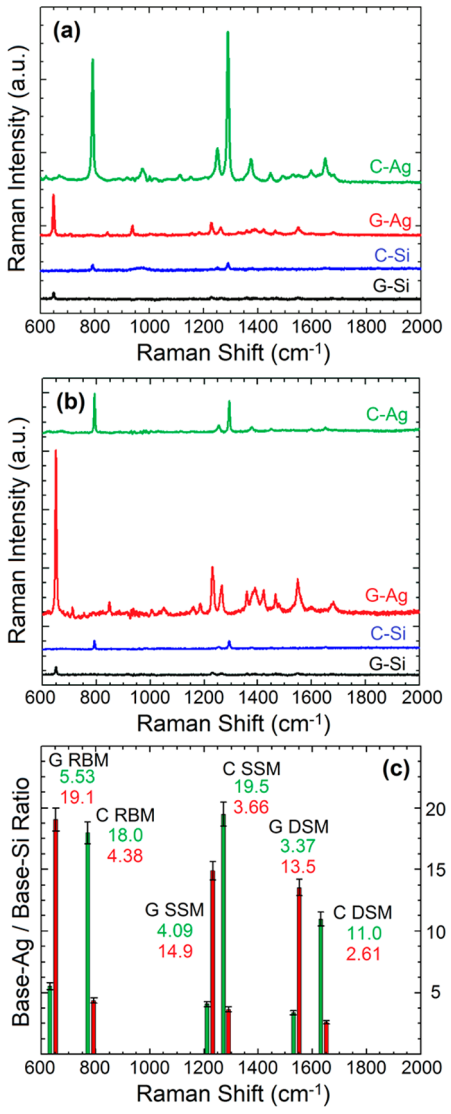

Figure 3. (a) Raman spectra of cytosine and guanine on Raman and SERS substrates with an excitation wavelength of 532 nm using substrate #1, with NRS measurements on silicon showing low Raman intensities and SERS measurements showing that C—Ag has a greater intensity than that of G—Ag. (b) Raman spectra of cytosine and guanine on Raman and SERS substrates with an excitation wavelength of 785 nm using substrate #2, with NRS measurements on silicon showing low Raman intensities and SERS measurements showing that G—Ag has a greater SERS intensity than that of C—Ag. (c) Bar graph displaying the ratios of Ag—Base to Si—Base at 532 nm (green) and 785 nm (red) excitation wavelengths for the guanine RBM (650 cm^{-1}), cytosine RBM (790 cm^{-1}), guanine SSM (1230 cm^{-1}), cytosine SSM (1290 cm^{-1}), guanine DSM (1550 cm^{-1}), and cytosine DSM (1650 cm^{-1}). The modes for cytosine have greater enhancement at 532 nm excitation, and the modes for guanine have greater enhancement at 785 nm excitation.

enhancement caused by the chemical enhancement, a resonance Raman effect. The NRS shows the RBM of C—Si and G—Si to have approximately the same intensity, as expected, due to the absence of silver and, thus, no charge-transfer resonance. The measured ratios of the Base—Ag to the Base—Si for all modes and wavelengths are shown in Figure 3c.

The ratios of the surface-enhanced Raman intensities (C−Ag, G−Ag) to the normal Raman scattering intensities (C−Si, G−Si) for the RBM, SSM, and DSM modes at both 532 nm (green) and 785 nm (red) excitation wavelengths give quantitative evidence that all modes are consistently higher for C−Ag at 532 nm and G−Ag at 785 nm. At 532 nm, C−Ag shows higher enhancement than G−Ag, with a RBM intensity ratio over C−Si and G−Si to be 18.0 and 5.53, respectively. At 785 nm, the opposite is seen as the ratio of RBM intensity of C−Ag to C−Si and G−Ag to G−Si are 4.38 and 19.1, respectively. The SSM and DSM results are also consistent with these findings. We conclude that this change in Raman intensity magnitude of the RBM, SSM, and DSM of the nucleic acids is caused by the presence of the nanoscale metal substrate, as the normal Raman scattering (NRS) shows approximately equivalent intensities of the RBMs for C−Si and G−Si at 532 nm (453 au and 454 au, respectively, in Figure 3a) and for C−Si and G−Si at 785 nm (301 au and 281 au, respectively, in Figure 3b). This further confirms that the discrepancy seen in literature in which nucleic acids have varying SERS intensities at different wavelengths while having the same NRS intensities at these wavelengths is caused by the charge-transfer between the metal and nucleic acid, known as the chemical enhancement effect of SERS.

To estimate this chemical enhancement effect, it is possible to sputter an atomic layer of aluminum oxide (Al_2O_3) *via* atomic layer deposition (ALD) on the metal nanostructures that will prevent electron transfer between the metal and molecules.[26] In this way, the chemical resonance effect would be removed as there would be no charge-transfer bands created by electron redistribution, causing a significant drop in the SERS intensities. Although Al_2O_3 or other thin films might cause a portion of the silver to oxidize and can be porous, researchers have successfully utilized Al_2O_3 for the elimination of the charge-transfer effect as well as for distance dependence studies, showing excellent correlation between simulations and experimental results.[27,28] The layer of aluminum oxide, compared to conventional thin film coatings, is actually highly stable to oxidation and temperature changes.

Previously published results have demonstrated the efficacy of using Al_2O_3 to measure the electromagnetic field decay as molecules move away from the surface. By adding several layers of Al_2O_3, Van Duyne *et al.* monitored the SERS intensity decay as the molecules were placed further away from the surface and experimentally measured the electromagnetic field strength as a function of distance from the surface.[29] In addition to the decrease caused by the distance between the nanostructure and molecule, there will also be a LSPR shift that will change the LSPR contribution. However, previous work has shown that only thick layers result in a substantial LSPR shift (~30 nm for 120 nm shift);[30] thus, an ultrathin layer will have a minimal impact on the LSPR shift.[27,31−33] On the basis of the successful demonstrations of using Al_2O_3 as a spacer layer, a 1 nm thick layer of aluminum oxide is assembled onto the substrates in order to eliminate the charge-transfer between the metal and molecules.

To calculate the dampening of the electromagnetic effect caused by a thin 1 nm layer of Al_2O_3 for silver island films, COMSOL simulations are performed on the previous COMSOL models (Figure 2a) with the addition of a 1 nm thick layer (Figure 4a). The 1 nm thick layer results in a decreased electromagnetic effect as the molecules rest 1 nm away from the maximum localized electric field. The simulation results show a decrease by 26.9% for substrate #1 and 23.0% for substrate #2, meaning the dampened plasmonic resonance will cause a moderate dip in the enhanced Raman signals. The simulation results agree well with previously published experimental measurements of the electromagnetic field decay caused by spacer layers.[28,29] Because the aluminum oxide prevents electron transfer and thus prevents a chemical enhancement from occurring, we expect to see a much more significant decrease in the Raman signals for substrates which previously demonstrated strong chemical enhancement (C−Ag at 532 nm, G−Ag at 785 nm).

As reported previously, the oxidation caused by this process will lead to a slight red shift of the λ_{LSPR} by ~13 nm,[33] which would slightly decrease the plasmonic resonance effect by roughly 10%. With the dampened plasmonic resonance and LSPR shift, we expect to see a decrease of ~30−40% when there is no chemical resonance present. If there is a chemical resonance, such as at 532 nm with C−Ag, we expect to see a much larger drop as new electronic transitions are not formed by the exchange of electrons. To measure the change in SERS intensity, 8 silver island film samples are prepared: 4 for 532 nm (substrate #1) and 4 for 785 nm (substrate #2). Two samples at each wavelength are sputtered with Al_2O_3 (1 with cytosine and 1 with guanine) and two are left clean without an Al_2O_3 layer. The resulting Raman measurements are shown in Figures 4b and 4c.

From the 532 nm (substrate #1) results (Figure 4b), the clean cytosine sample shows a high RBM magnitude. When a 1 nm thick Al_2O_3 layer is added to the surface, this intensity decreases by 83.4%, which is a much higher drop than expected and is caused by the elimination of the charge-transfer band that leads to a chemical enhancement. However, for guanine, which sees a weak chemical enhancement at 532 nm, the 1 nm thick layer only causes a RBM Raman intensity decrease by 48.3% compared to the clean guanine sample, which agrees well with the effect on the plasmonic resonance caused by distance dependence and elimination of a weak chemical resonance. For the 785 nm results (substrate #2, Figure 4c), the opposite is

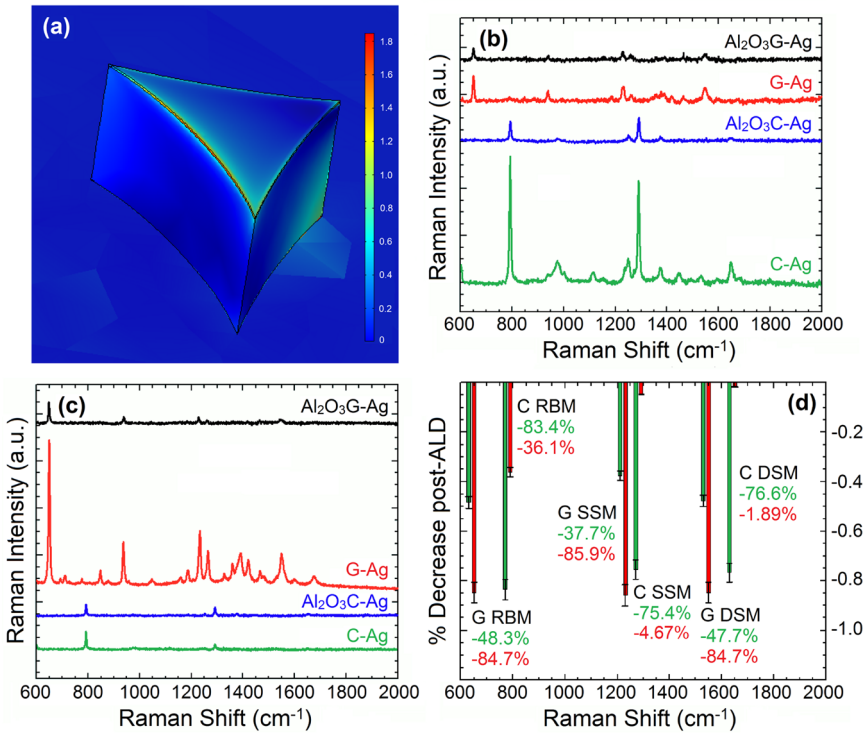

Figure 4. (a) COMSOL results of 1 nm thick Al_2O_3 layer on silver island films showing a moderate decrease in intensity of localized electric field. (b) SERS results of cytosine and guanine at an excitation wavelength of 532 nm (substrate #1) with a clean sample and a sample with an aluminum oxide coating. C−Ag shows a much larger drop with the addition of the aluminum oxide layer. (c) SERS results of cytosine and guanine at an excitation wavelength of 785 nm (substrate #2) with a clean sample and a sample with an aluminum oxide coating. Unlike at 532 nm, G−Ag shows a much larger drop than that of C−Ag after ALD. (d) Bar graph displaying the percent decrease in Raman intensities of the RBM, SSM, and DSM of cytosine and guanine after addition of atomic layer of aluminum oxide. G−Ag modes show much larger drops with the 785 nm excitation wavelength (red), and C−Ag modes show much larger drops with the 532 nm excitation wavelength (green). This correlates with our findings, as the atomic layer prevents electron transfer and leads to a more dramatic decrease in Raman intensity for substrates that previously displayed strong chemical resonances.

seen as the guanine Al_2O_3 measurement decreases by 84.7% compared to the clean sample and the cytosine Al_2O_3 measurement decreases by 36.1% compared to the clean sample. This confirms that cytosine does not have a strong chemical enhancement at 785 nm, but guanine does. A summary of the percent decrease for all Raman modes can be found in Figure 4d. The SSM and DSM of cytosine at 785 nm have the least amount of percent change when adding the atomic layer of aluminum oxide because these modes lie further from the excitation line (1290 and 1650 cm^{-1}). On the basis of the values in Figure 4d, the chemical enhancement appears to be less than 10, which correlates well to previously published research results.[34] Although this value seems low, it leads to a dramatic difference in Raman spectra, particularly because the plasmonic resonance will always have the same order of magnitude effect on different molecules. The chemical resonance, since it varies from molecule to molecule, can lead to drastic differences in the SERS signal and thus can make some molecules undetectable.

CONCLUSIONS

In this paper, we have shown that the charge-transfer mechanism has been responsible for the failure to obtain accurate SERS measurements on DNA bases, as well as the inability to perform SM-SERS measurements on nucleic acids other than adenine. We have successfully demonstrated that new electronic states of nucleic acid silver systems are created in the visible range and differ for different nucleic acid metal systems. We then experimentally verified the creation of new electronic transitions by performing optical absorption measurements on cytosine and guanine attached to silver. We showed that by tuning the excitation frequency, the enhancement of the SERS signal for C−Ag and G−Ag will change based on the charge-transfer bands of each molecule-metal system being resonant with the excitation frequency. These results confirm that the variance of the SERS signal in nucleic acids comes from the charge-transfer mechanism, rather than differences in the Raman cross section or orientation of the molecules. This chemical enhancement effect can vary dramatically for two similar molecules, as seen with cytosine and guanine. By identifying the reason for amplification differentiation, we believe that future work would enable all nucleic acids to be measured using SERS by tuning the excitation wavelength. With additional TD-DFT studies and optical absorption measurements on the other nucleic

acids in conjunction with these results, we predict that it will be possible to perform SM-SERS when the excitation energy is appropriately optimized for the nucleic acid in question.

Broadband SERS substrates or multiresonance SERS substrates can be utilized as tools for achieving the amplified SERS charge-transfer band intensities at multiple wavelengths and thus will be the focus of our future work. Only two nucleic acids were chosen for this work to simplify the results, so future work must also take into account the other two nucleic acids (adenine and thymine). While there are many challenges that remain for a Raman based sequencing method such as spatial resolution and poor signal-to-noise ratio (SNR) which can be addressed by statistical analysis, the issue of surface-enhanced Raman intensity can be resolved as being wavelength dependent and caused by the charge-transfer resonances of the system.

METHODS

For TD-DFT simulations, B3LYP (Becke, 3-parameter, Lee–Yang–Parr)[35] is chosen as the DFT method as it employs both generalized gradient approximations and local-density approximations that are suitable for molecule-metal systems.[36,37] On the basis of the molecular structures, a 6-31G(d,p) basis set is used for the isolated nucleic acids and a split basis set of 6-31G(d,p) and LANL2DZ is used for the nucleic acid molecules and silver atoms, respectively, for the DNA base metal systems.

COMSOL simulations with silver islands are modeled in an air environment (refractive index $n = 1$) on a silicon substrate ($n = 3.5$) with light propagation in the z-direction using incident wavelengths of 532 nm (1) and 785 nm (2) and an initial unpolarized electric field strength of 1 V/m. A spherical perfectly matched layer (PML) with a radius of 1 μm and a thickness of 200 nm absorbs scattered light. The silver islands and 1 nm thick layer of aluminum oxide use extremely fine meshing and all other elements use fine meshing.

Optical absorption and scattering spectra are recorded using a broadband UV–visible fiber optic illuminator and spectrometer (Ocean Optics HR4000). Spectra are normalized with respect to the background silicon signal. Five spectra are taken for scattering measurements, and the mean intensity is plotted with respect to wavelength. Error bars represent the standard deviation of the five intensity measurements.

For SERS measurements, cytosine and guanine (VWR International) are dissolved in H_2O for resulting concentrations of 3 mM. This solution is then drop coated on the 1 cm^2 silver island film substrates (substrate #1 and #2) and allowed to be incubated overnight. The samples are then rinsed to remove bulk unattached nucleic acids on the surface, leaving behind approximately a monolayer of adsorbed cytosine or guanine molecules on the silver islands.

SERS Measurements. Raman spectroscopy is performed using a Renishaw Raman spectrometer at the wavelengths of 532 and 785 nm. Spectra are recorded using the hyperSpec program. The sample is imaged using a 40× objective, and the area which data are acquired is confirmed to contain silver island films with nucleic acids by using markers and SEM verification. The laser power of each wavelength is calibrated by comparing the intensity of the 500 cm^{-1} mode of a Si wafer. A 10 s acquisition time is used with a Raman spectral range of 600–2000 cm^{-1} to eliminate the 500 cm^{-1} line from Si. Baseline subtraction is then performed to ensure that all spectra are level with the x-axis.

Aluminum oxide is sputtered onto the silver island films using ALD (Beneq TFS200, Calit2 Nano3 Cleanroom, UCSD) to a thickness of 0.99 nm in order to eliminate the chemical enhancement effect. Trimethylaluminum (TMA) and H_2O vapors are alternatively pulsed through the chambers at a temperature of 250 °C with an average rate of 0.9 Å/cycle for 11 cycles.

Conflict of Interest: The authors declare no competing financial interest.

Acknowledgment. The authors thank M. J. Sailor (Department of Chemistry and Biochemistry, UCSD) for the use of his Renishaw Raman spectrometer. This work was supported by DARPA, the NSF, through the Center for Integrated Access Networks (CIAN) ERC, the Cymer Corporation, the Army Research Office, and the Office of Naval Research MURI.

REFERENCES AND NOTES

1. Davies, K. *The $1,000 Genome: The Revolution in DNA Sequencing and the New Era of Personalized Medicine (Google eBook)*; Simon and Schuster: New York, NY, 2010; p 352.
2. Kelly, K. L.; Coronado, E.; Zhao, L. L.; Schatz, G. C. The Optical Properties of Metal Nanoparticles: The Influence of Size, Shape, and Dielectric Environment. *J. Phys. Chem. B* **2003**, *107*, 668–677.
3. Gopinath, A.; Boriskina, S. V.; Reinhard, B. M.; Dal Negro, L. Deterministic Aperiodic Arrays of Metal Nanoparticles for Surface-Enhanced Raman Scattering (SERS). *Opt. Express* **2009**, *17*, 3741.
4. Emory, S. R.; Nie, S. Screening and Enrichment of Metal Nanoparticles with Novel Optical Properties. *J. Phys. Chem. B* **1998**, *102*, 493–497.
5. Wang, S.; Pile, D. F. P.; Sun, C.; Zhang, X. Nanopin Plasmonic Resonator Array and Its Optical Properties. *Nano Lett.* **2007**, *7*, 1076–1080.
6. Su, K.-H.; Durant, S.; Steele, J. M.; Xiong, Y.; Sun, C.; Zhang, X. Raman Enhancement Factor of a Single Tunable Nanoplasmonic Resonator. *J. Phys. Chem. B* **2006**, *110*, 3964–3968.
7. Chen, H. M.; Pang, L.; King, A.; Hwang, G. M.; Fainman, Y. Plasmonic Coupled Nanotorch Structures Leading to Uniform Surface Enhanced Raman Scattering Detection. *Nanoscale* **2012**, *4*, 7664–7669.
8. Otto, C.; van den Tweel, T.; de Mul, F.; Greve, J. Surface-Enhanced Raman Spectroscopy of DNA Bases. *J. Raman Spectrosc.* **1986**, *17*, 289–298.
9. Kneipp, K.; Kneipp, H.; Kartha, V.; Manoharan, R.; Deinum, G.; Itzkan, I.; Dasari, R.; Feld, M. Detection and Identification of a Single DNA Base Molecule Using Surface-Enhanced Raman Scattering (SERS). *Phys. Rev. E* **1998**, *57*, R6281–R6284.
10. Lagally, E. T.; Medintz, I.; Mathies, R. A. Single-Molecule DNA Amplification and Analysis in an Integrated Microfluidic Device. *Anal. Chem.* **2001**, *73*, 565–570.
11. McNay, G.; Eustace, D.; Smith, W. E.; Faulds, K.; Graham, D. Surface-Enhanced Raman Scattering (SERS) and Surface-Enhanced Resonance Raman Scattering (SERRS): A Review of Applications. *Appl. Spectrosc.* **2011**, *65*, 825–837.
12. Green, M.; Liu, F.-M.; Cohen, L.; Kollensperger, P.; Cass, T. SERS Platforms for High Density DNA Arrays. *Faraday Discuss.* **2006**, *132*, 269.
13. Barhoumi, A.; Zhang, D.; Tam, F.; Halas, N. J. Surface-Enhanced Raman Spectroscopy of DNA. *J. Am. Chem. Soc.* **2008**, *130*, 5523–5529.
14. Yamada, H.; Nagata, H.; Toba, K.; Nakao, Y. Charge-Transfer Band and SERS Mechanism for the Pyridine-Ag System. *Surf. Sci.* **1987**, *182*, 269–286.
15. Sun, M.; Liu, S.; Chen, M.; Xu, H. Direct Visual Evidence for the Chemical Mechanism of Surface-Enhanced Resonance Raman Scattering *via* Charge Transfer. *J. Raman Spectrosc.* **2009**, *40*, 137–143.
16. Sun, M.; Wan, S.; Liu, Y.; Jia, Y.; Xu, H. Chemical Mechanism of Surface-Enhanced Resonance Raman Scattering *via* Charge Transfer in pyridine–Ag2 Complex. *J. Raman Spectrosc.* **2008**, *39*, 402–408.

17. Valley, N.; Greeneltch, N.; Van Duyne, R. P.; Schatz, G. C. A Look at the Origin and Magnitude of the Chemical Contribution to the Enhancement Mechanism of Surface-Enhanced Raman Spectroscopy (SERS): Theory and Experiment. *J. Phys. Chem. Lett.* **2013**, *4*, 2599–2604.
18. Huang, R.; Yang, H.-T.; Cui, L.; Wu, D.-Y.; Ren, B.; Tian, Z.-Q. Structural and Charge Sensitivity of Surface-Enhanced Raman Spectroscopy of Adenine on Silver Surface: A Quantum Chemical Study. *J. Phys. Chem. C* **2013**, *117*, 23730–23737.
19. Huang, R.; Zhao, L.-B.; Wu, D.-Y.; Tian, Z.-Q. Tautomerization, Solvent Effect and Binding Interaction on Vibrational Spectra of Adenine−Ag + Complexes on Silver Surfaces: A DFT Study. *J. Phys. Chem. C* **2011**, *115*, 13739–13750.
20. Chong, D. P. *Recent Advances in Density Functional Methods*; World Scientific: River Edge, NJ, 1995.
21. Andzelm, J.; Wimmer, E. Density Functional Gaussian-Type-Orbital Approach to Molecular Geometries, Vibrations, and Reaction Energies. *J. Chem. Phys.* **1992**, *96*, 1280.
22. Soto-Verdugo, V.; Metiu, H.; Gwinn, E. The Properties of Small Ag Clusters Bound to DNA Bases. *J. Chem. Phys.* **2010**, *132*, 195102.
23. Jensen, T. R.; Malinsky, M. D.; Haynes, C. L.; Van Duyne, R. P. Nanosphere Lithography: Tunable Localized Surface Plasmon Resonance Spectra of Silver Nanoparticles. *J. Phys. Chem. B* **2000**, *104*, 10549–10556.
24. Kats, M. A.; Yu, N.; Genevet, P.; Gaburro, Z.; Capasso, F. Effect of Radiation Damping on the Spectral Response of Plasmonic Components. *Opt. Express* **2011**, *19*, 21748–21753.
25. Zuloaga, J.; Nordlander, P. On the Energy Shift between Near-Field and Far-Field Peak Intensities in Localized Plasmon Systems. *Nano Lett.* **2011**, *11*, 1280–1283.
26. Stiles, P. L.; Dieringer, J. a; Shah, N. C.; Van Duyne, R. P. Surface-Enhanced Raman Spectroscopy. *Annu. Rev. Anal. Chem.* **2008**, *1*, 601–626.
27. Zhang, X.; Zhao, J.; Whitney, A. V.; Elam, J. W.; Van Duyne, R. P. Ultrastable Substrates for Surface-Enhanced Raman Spectroscopy: Al_2O_3 Overlayers Fabricated by Atomic Layer Deposition Yield Improved Anthrax Biomarker Detection. *J. Am. Chem. Soc.* **2006**, *128*, 10304–10309.
28. Willets, K. A.; Van Duyne, R. P. Localized Surface Plasmon Resonance Spectroscopy and Sensing. *Annu. Rev. Phys. Chem.* **2007**, *58*, 267–297.
29. Dieringer, J. A.; McFarland, A. D.; Shah, N. C.; Stuart, D. A.; Whitney, A. V.; Yonzon, C. R.; Young, M. A.; Zhang, X.; Van Duyne, R. P. Introductory Lecture: Surface Enhanced Raman Spectroscopy: New Materials, Concepts, Characterization Tools, and Applications. *Faraday Discuss.* **2006**, *132*, 9.
30. Murray, W. A.; Suckling, J. R.; Barnes, W. L. Overlayers on Silver Nanotriangles: Field Confinement and Spectral Position of Localized Surface Plasmon Resonances. *Nano Lett.* **2006**, *6*, 1772–1777.
31. John, J. F.; Mahurin, S.; Dai, S.; Sepaniak, M. J. Use of Atomic Layer Deposition to Improve the Stability of Silver Substrates for in situ, High-Temperature SERS Measurements. *J. Raman Spectrosc.* **2010**, *41*, 4–11.
32. Whitney, A. V.; Elam, J. W.; Zou, S.; Zinovev, A. V.; Stair, P. C.; Schatz, G. C.; Van Duyne, R. P. Localized Surface Plasmon Resonance Nanosensor: A High-Resolution Distance-Dependence Study Using Atomic Layer Deposition. *J. Phys. Chem. B* **2005**, *109*, 20522–20528.
33. Chan, G. H.; Zhao, J.; Schatz, G. C.; Duyne, R. P. Van. Localized Surface Plasmon Resonance Spectroscopy of Triangular Aluminum Nanoparticles. *J. Phys. Chem. C* **2008**, *112*, 13958–13963.
34. Zayak, A. T.; Choo, H.; Hu, Y. S.; Gargas, D. J.; Cabrini, S.; Bokor, J.; Schuck, P. J.; Neaton, J. B. Harnessing Chemical Raman Enhancement for Understanding. *J. Phys. Chem. Lett.* **2012**, *3*, 1357–1362.
35. Becke, A. D. A New Mixing of Hartree−Fock and Local Density-Functional Theories. *J. Chem. Phys.* **1993**, *98*, 1372.
36. Muniz-Miranda, M.; Pergolese, B.; Bigotto, A. SERS and DFT Study of Nitroarenes Adsorbed on Metal Nanoparticles. *Vib. Spectrosc.* **2007**, *43*, 97–103.
37. Zhang, L.; Fang, Y.; Zhang, P. Experimental and DFT Theoretical Studies of SERS Effect on Gold Nanowires Array. *Chem. Phys. Lett.* **2008**, *451*, 102–105.